Vibrations of quantum dots and light scattering properties: Atomistic versus continuous models

Nicolas Combe,* Jean Roch Huntzinger,† and Adnen Mlayah‡
Centre d'Elaboration de Matériaux et d'Etudes Structurales, CNRS UPR 8011, 29 Rue J. Marvig, Boîte Postale 94347, 31055 Toulouse Cedex 4, France
(Received 13 June 2007; published 20 November 2007)

The resonant inelastic light scattering by acoustic vibration modes in spherical germanium nanocrystals is studied theoretically. The Raman-Brillouin efficiency is calculated using quantum perturbation theory and assuming deformation-potential interaction between the confined electronic states and the nanocrystal vibration modes. The electronic states are described using the effective mass approximation. The vibration modes are calculated, on one hand, using an atomistic approach based on the Stillinger-Weber interaction potential and, on the other hand, using elasticity theory (Lamb's model). Both models are compared depending on the nanocrystal size and on the surface boundary conditions. By projecting the Stillinger-Weber vibration modes on Lamb's modes, we are able to discuss the validity of the elasticity theory and to determine the origin of the low-frequency Raman-Brillouin scattering.

DOI: 10.1103/PhysRevB.76.205425 PACS number(s): 78.67.Hc, 78.30.−j, 63.20.Kr, 63.22.+m

I. INTRODUCTION

The vibration properties of quantum dots (QDs) and their related Raman activity is the subject of a continuous interest because fundamental questions related to the localized and discrete nature of the electronic and vibronic density of states are still open.

The vibration eigenmodes of a QD embedded in a matrix having similar acoustic properties are bulklike phonons extending over distances much larger than the QD size. This is the case, for instance, of Si/Ge, GaAs/AlAs, and InAs/InP quantum dots. In these systems, the interactions between localized electronic states and extended acoustic waves show interference effects in the Raman scattering[1–10]

On the contrary, semiconductor [CdS (Refs. 11–13), Si (Refs. 14–17), and Ge (Refs. 18–20)] and noble metal nanoparticles [Ag (Refs. 21–26) and Au (Refs. 25 and 27)] embedded in glass or polymers show localized acoustic vibrations.[28–30] Whereas the elasticity theory well describes bulklike long-wavelength acoustic waves, its validity becomes questionable in the case of vibrations localized in very small QDs: Up to which QD size is elasticity theory (Lamb's model) able to describe the vibration eigenfrequencies and eigenmodes of quantum dots? What is the connection between the confined acoustic modes calculated using elasticity theory and those obtained using an atomistic approach? Is the Raman scattering activity of elastic modes different from that of atomistic modes? These are some of the questions addressed in this work.

The validity of elasticity theory has been discussed already in the 1980s: for instance, Tamura and Ichinokawa[31] compared the vibration spectra obtained from elasticity theory and molecular dynamics of small particles (hundreds of argon atoms). They showed that the elastic body approximation well describes the vibration frequencies providing that some parameters reflecting the symmetry and periodicity of the real lattice are included.

Recently, Leonforte and co-workers considered this problem for amorphous materials.[32–34] They found that elasticity theory breaks down below a surprisingly large length scale of about 23 molecular sizes. Cheng *et al.*[35–37] recently studied the size dependence of the vibration density of states of freestanding germanium and silicon nanocrystals using a two parameter (bond stretching and bond bending) valence force field (VFF) model. By projecting Lamb's modes on the VFF vibration modes, they showed that Lamb's model (and thus elasticity theory) starts to break down for a quantum dot with a diameter less than 4 nm. In addition, the vibration density of states of such small QDs is dominated by surface modes whose frequency is size independent.

Calculations of Raman scattering efficiency require the modeling of both electronic states and vibration modes as well as their interaction mechanisms. In order to do so, an atomistic description of the vibration modes and first-principles calculations of the electronic states are needed. Most of the reported studies using atomistic calculations of the vibration eigenmodes use a bond polarizability model[38,39] to generate the Raman spectra. This model does not explicitly take into account the electronic states. However, based on symmetry arguments and using few adjustable parameters, it gives a good description of the off-resonance Raman spectra. For this reason, this approach has been widely used in the literature.[35,40–42]

On the other hand, only few attempts to include the electronic states in the calculation of the resonant Raman scattering have been reported. Since first-principles calculations (Hartree-Fock, density functional theory, or time-dependent density functional theory) can only treat a limited number of atoms, people have used the envelope function approximation[43] and/or effective mass approximation[44] to overcome this limitation. Sirenko *et al.*[45] considered the deformation-potential interaction of bulklike acoustic phonons with confined electronic states to calculate the Raman scattering of embedded CdS nanocrystals. Chamberlain *et al.*[46] considered the Fröhlich interaction of confined optical phonons with confined electron-hole states. Gupalov and Merkulov[47] calculated the line shape and polarization properties of the acoustic phonon Raman scattering, including the complex structure of the electronic states due to confinement and spin-orbit interaction. Recently,[48] some of us have reported on resonant Raman scattering in embedded germa-

nium QDs. The vibration modes were calculated in the frame of elasticity theory, but only the contribution of pure radial modes was considered.

In this work, we combine both an atomistic description of the QD vibration modes and a quantum description of the light scattering in order to study the influence of the atomistic approach on the vibration mode frequencies and eigenvectors and on their resonant Raman spectra.

Calculations of the Raman scattering efficiency are performed for vibration modes obtained from both atomistic and elastic models. The general framework of this calculation is given in Sec. II. Section III details the calculation of the vibration eigenmodes using both the atomistic (Sec. III A) and the elastic models (Sec. III B). The electronic states as well as the electron-phonon coupling are obtained using the general formalism described in Sec. IV. In Sec. V, the atomistic and elastic descriptions are compared by inspecting both the vibration modes and their Raman spectra. The rules for the Raman activity naturally come out from our calculations. They are discussed and compared to experimental data and to theoretical predictions from the literature. Finally, size effects are considered. The results are obtained for both stress free and blocked surface boundary conditions. In Sec. VI the validity of the different approximations is discussed.

II. RAMAN-BRILLOUIN SCATTERING EFFICIENCY

The resonant Raman scattering efficiency is calculated using third order perturbation theory. The probability per unit time for an incident photon to get inelastically scattered through a Raman process is dominated by the resonant term,[49]

$$R_{fi} = \frac{1}{\hbar}\sum_{phonon}\left|\sum_{k,l}\frac{\langle\eta_f|H_\nu^s(\omega_{scatter})|\eta_k\rangle}{(\hbar w_{ki}-\hbar\omega_{inc}\pm\hbar\Omega-i\Gamma_k)}\times\langle\eta_k|H_{ph}|\eta_l\rangle\frac{\langle\eta_l|H_\nu^i(\omega_{inc})|\eta_i\rangle}{(\hbar w_{li}-\hbar\omega_{inc}-i\Gamma_l)}\right|^2\times\delta(\hbar\omega_{scatter}\pm\hbar\Omega-\hbar\omega_{inc}), \quad (1)$$

where Ω, ω_{inc}, and $\omega_{scatter}$ are the frequencies of the vibration mode, the incident and scattered photons, respectively. The double sum $\Sigma_{k,l}$ in Eq. (1) runs over all electronic eigenstates. H_{ph}, H_ν^s, and H_ν^i are, respectively, the electron-phonon, electron-scattered photon, and electron-incident photon Hamiltonians. For a phonon creation (absorption), i.e., a Stokes (anti-Stokes) process, the $\pm$ sign of Eq. (1) must be replaced by + (−). Wave functions $|\eta\rangle=|\phi\rangle\otimes|\Psi\rangle$ describing quantum states have an electronic and a nuclear part: $|\phi\rangle$ and $|\Psi\rangle$, respectively. The final electronic state $|\phi_f\rangle$ of $|\eta_f\rangle=|\phi_f\rangle\otimes|\Psi_f\rangle$ has to be the same as $|\phi_i\rangle$ of the initial state $|\eta_i\rangle=|\phi_i\rangle\otimes|\Psi_i\rangle$ because in a Raman process it is the excited electron-hole pair that recombines after phonon emission or absorption (geminate recombination). $|\Psi_i\rangle$ and $|\Psi_f\rangle$ are initial and final states of the phonon bath. Finally, $\hbar w_{li}=E_l-E_i$, where E_l is the energy of electronic state $|\phi_l\rangle$ and Γ_l is its homogeneous broadening.[50] In this paper, all Γ_l have been fixed to 1 cm^{-1}. For a detailed study of the homogeneous broadening on the Raman intensity see Ref. 48. Our aim is to generate the Raman spectra of all the QD's vibration modes using Eq. (1). The latter are obtained following two approaches: on one hand, using Lamb's model,[51] and, on the other hand, using an atomistic description of the interaction between atoms based on the Stillinger-Weber (SW) empirical potential.[52–55]

III. VIBRATION EIGENMODES

A. Atomistic description

1. Eigenstates

A judicious basis for the nuclear states $|\Psi\rangle$ can be obtained by diagonalizing the unperturbed Hamiltonian,

$$H_0^{\mathcal{N}} = \sum_{i=0}^{N-1}\frac{\vec{p}_i^{\,2}}{2m_i} + \sum_{i,j=0;\alpha,\beta\in\{x,y,z\}}^{N-1}\frac{1}{2}\frac{\partial^2 V_{\mathcal{N}\mathcal{N}}}{\partial u_i^\alpha \partial u_j^\beta}u_i^\alpha u_j^\beta, \quad (2)$$

where $V_{\mathcal{N}\mathcal{N}}$ is the interatomic potential, $\vec{p}_i$, m_i, and $\vec{u}_i$ are, respectively, momentum, mass, and displacement vector of nucleus i from its equilibrium position. Changing coordinates $\vec{u}_i'$ to $\sqrt{m_i}\vec{u}_i$ and, thus, the conjugate momentum $\vec{p}_i'$ to $\vec{p}_i/\sqrt{m_i}$, $H_0^{\mathcal{N}}$ reads

$$H_0^{\mathcal{N}} = \sum_{i=0}^{N-1}\frac{\vec{p}_i'^{\,2}}{2} + \sum_{i,j=0;\alpha,\beta\in\{x,y,z\}}^{N-1}\frac{1}{2\sqrt{m_i}\sqrt{m_j}}\frac{\partial^2 V_{\mathcal{N}\mathcal{N}}}{\partial u_i^\alpha \partial u_j^\beta}u_i'^{\alpha}u_j'^{\beta} \quad (3)$$

$$= \sum_{l=0}^{3N-1}\frac{p_l'^{\,2}}{2} + \sum_{k,l=0}^{3N-1}\frac{1}{2}B[k,l]u_k'u_l', \quad (4)$$

where $B[k,l]=\frac{1}{\sqrt{m_i}\sqrt{m_j}}\frac{\partial^2 V_{\mathcal{N}\mathcal{N}}}{\partial u_i^\alpha \partial u_j^\beta}$ is the *dynamical matrix*. l stands for $3i+\alpha$, where i is the atom number and $\alpha=0$, 1, or 2 denotes x, y, or z direction. In the following, we will only use the extended coordinates l: m_l will thus refer to m_i such that $l=3i+\alpha$. $B[k,l]$ is a symmetric real matrix by construction. It can thus be diagonalized in real space. Let $P[k,l]$ be the matrix formed by the *normalized* eigenvectors of B. Then, we have $P^{-1}BP=\mathrm{diag}[\lambda_0\cdots\lambda_{3N-1}]$, where λ_l is an eigenvalue of B and $\Omega_l=\sqrt{\lambda_l}$ the eigenfrequency. Let Θ_l be the normal coordinate $\Theta_l=\Sigma_k P^{-1}[l,k]u_k'$, and Π_l its conjugate momentum; $H_0^{\mathcal{N}}$ now reads

$$H_0^{\mathcal{N}} = \sum_{l=0}^{3N-1}\left[\frac{\Pi_l^2}{2}+\frac{\Omega_l^2}{2}\Theta_l^2\right], \quad (5)$$

which is the Hamiltonian of $3N$ uncoupled harmonic oscillators.

The normalization of the vibration eigenmodes is often discussed in the literature and is sometimes misunderstood. Our diagonalization procedure prevents any mistake concerning that point: The normalization is imposed by the condition that P is a unitary matrix, and therefore $P^tP={}^tPP=I$. The displacement field operator of atom i reads (see the Appendix),

$$u_l = \sum_{k=0}^{3N-1} P[l,k] \sqrt{\frac{\hbar}{2\Omega_k m_l}} (a_k^\dagger + a_k), \tag{6}$$

where $a_k^\dagger$ and a_k are, respectively, the creation and annihilation operators of vibration mode k.

2. Semiempirical potential

To use Eq. (6), one needs the P matrix and the eigenfrequencies Ω_l. We calculate the vibration modes of spherical nanoparticles whose atoms (germanium) form a diamond crystal structure. The interatomic interaction is described by a SW potential.[52–55] This semiempirical potential has been designed for semiconductors and contains a pair potential and three-body interaction terms. The parameters used in this work are from the original papers.[52,53] We first relax the nanoparticle strain by minimizing the overall potential energy using the conjugate gradient algorithm. This procedure ensures that all vibration eigenfrequencies are real. Our model omits the possible existence of surface reconstructions and dangling bonds. These aspects could correctly be addressed using more sophisticated techniques (for instance, density functional theory or tight binding). Concerning the elastic stress at the nanoparticle surface, two limiting cases are studied here: (i) stress free (SF), where the nanoparticle moves freely in vacuum, and (ii) blocked surface (BS), where the surface atoms are fixed, a situation which corresponds to a nanoparticle embedded in a rigid matrix.

We calculate the dynamical matrix B defined in Eq. (4) from the analytic expression of the potential energy. B is diagonalized to obtain the eigenfrequencies Ω_l, the eigenvectors, and hence the P matrix (Sec. III A 1). We would like to underline that the dynamical matrix is here diagonalized without any assumption concerning the symmetry of the eigenmodes.[36,37] Moreover, we checked that all eigenvalues are real and positive.

B. Lamb's model: Elasticity theory

Lamb[51] has described the vibration modes of an elastic and isotropic homogeneous free sphere using elasticity theory. The displacement vector $\vec{u}$ is obtained from the Navier-Stokes equation,

$$\frac{\partial^2 \vec{u}}{\partial t^2} = v_L^2 \,\vec{\text{grad}}[\text{div}\,\vec{u}] + v_T^2 \,\vec{\text{rot}}\,\vec{\text{rot}}\,\vec{u}. \tag{7}$$

The vibration properties are described by only two independent parameters, v_L and v_T, the longitudinal and transverse sound velocities, respectively. In spherical coordinates, the displacement field $\vec{u}$ reads

$$\begin{aligned}\vec{u}_{n,l,m} = {} & A_{n,l,m}\,\vec{\text{grad}}[j_l(Q^L_{n,l,m} r) Y_{lm}(\theta,\phi)] \\ & + B_{n,l,m}\,\vec{\text{rot}}[j_l(Q^T_{n,l,m} r) Y_{lm}(\theta,\phi)\vec{r}] \\ & + C_{n,l,m}\,\vec{\text{rot}}\,\vec{\text{rot}}[j_l(Q^T_{n,l,m} r) Y_{lm}(\theta,\phi)\vec{r}],\end{aligned} \tag{8}$$

where n, l, and m are integers, j_l are the spherical Bessel functions, and Y_{lm} are the spherical harmonics. $Q^L_{n,l,m}$ and $Q^T_{n,l,m}$ define the dispersion relations

$$Q^L_{n,l,m} = \frac{\Omega_{n,l,m}}{v_L}, \tag{9}$$

$$Q^T_{n,l,m} = \frac{\Omega_{n,l,m}}{v_T}. \tag{10}$$

The first and third terms of Eq. (8) are associated with spheroidal modes. The second term is for pure torsional modes. The dispersion relations and continuity of the displacement and stress fields at the nanoparticle surface allow us to calculate the eigenfrequencies $\Omega_{n,l,m}$ and to obtain the amplitudes $A_{n,l,m}$, $B_{n,l,m}$, and $C_{n,l,m}$. As will be discussed later, the electron-phonon interaction Hamiltonian is proportional to the dilation associated with the displacement field (divergence). Thus, pure transverse modes are not Raman actives, and hence modes with only $B \neq 0$ will not be considered here. In order to compare vibration modes and Raman spectra calculated using the atomistic description and elasticity theory, we obtain the longitudinal and transverse sound velocities in the $\langle 100 \rangle$ and $\langle 111 \rangle$ directions by applying our atomistic model to bulk germanium. The average sound velocities are then calculated following the procedure described in Ref. 48. We obtain $v_T = 3410$ m s^{-1} and $v_L = 5498$ m s^{-1}. These values are close to the experimental ones:[37] $v_T = 3250$ m s^{-1} and $v_L = 5250$ m s^{-1}. Moreover, for a given Lamb mode, the displacement of each atom of the atomistic model is calculated using Eq. (8). As for the atomistic description, this vector is normalized (see the Appendix). This gives the Lamb eigenvectors. In order to compare the atomistic description and the Lamb theory, both eigenvectors in matrix P (see Sec. III A 2) and Lamb eigenvectors will undergo the same treatment.

IV. ELECTRONIC STATES

A. Wave functions

The electronic states are described in the frame of the effective mass approximation, assuming parabolic band[56] dispersion. We emphasize the fact that a complete theory of resonant Raman scattering would require a correct description of the electronic states, including excited states, using, for instance, first-principles calculations. The drawback of such theories is, of course, the computational cost which forbids the calculation of the Raman intensities of a thousand atoms. Nevertheless, in this work, our aim is to study the influence of an atomistic description of the vibrational modes on the Raman spectra and to compare with the predictions based on elasticity theory. Furthermore, the Raman scattering efficiency calculated using an atomistic description of the vibration modes usually involves a Raman tensor based on the bond polarizability model.[36–38] This approach is very useful for the interpretation of Raman experiments performed with an optical excitation energy away from any electronic transition, whereas the experiments on nanocrystals are usually performed under resonant excitation in order to overcome the very low scattering volume. Hence, our model, though very simple for the description of the electronic states, allow us to simulate resonant Raman spectra,

which could be compared to available experimental data.

In addition to the effective mass approximation, we use the envelope function approximation.[43,44] Electronic wave functions are $\phi(\vec{r})=\zeta(\vec{r})u_{Bloch}(\vec{r})$, where ζ is the slowly varying envelope wave function and u_{Bloch} a Bloch function. We assume that the electronic states could be described using a single u_{Bloch} function. For a spherical nanocrystal of radius a with an infinite confining potential well, the envelope wave functions of electrons (and holes) read:[46]

$$\zeta_{nlm}(\vec{r}) = \frac{1}{j_{l+1}(\kappa_{n,l})}\sqrt{\frac{2}{a^3}}j_l\left(\kappa_{n,l}\frac{r}{a}\right)Y_{lm}(\theta,\phi), \tag{11}$$

where $\kappa_{n,l}$ is the nth zero of the spherical Bessel function $j_l(r)$. $Y_{lm}(\theta,\phi)$ are spherical harmonic functions. The quantized energies are given by

$$E_{n,l} = \frac{\hbar^2}{2m^*}\left(\frac{\kappa_{n,l}}{a}\right)^2, \tag{12}$$

where m^* is the effective mass of the electron or hole.

Since most of the published Raman experiments on Ge nanocrystals were performed under resonant excitation of the confined E_1 transitions, we shall consider, in the following, electronic transitions between valence and conduction states of germanium around the E_1 band gap. As shown by Cardona and Pollack,[57,58] the energy-band structure around the E_1 band gap of Ge is actually more complex than a simple parabola and is much better described by the $\mathbf{k}\cdot\mathbf{p}$ theory. Moreover, in order to calculate the Raman selection rules (polarization dependence), one should take into account the mixing of states with different envelope angular momenta.[59] Our description of the QD electronic states could thus be greatly improved, but is acceptable since our aim is to focus on the vibrational dynamics description and its consequences on the simulations of resonant Raman spectra.

In addition, the high joint density of states at the E_1 point is here taken into account by considering infinite effective masses. $E_{n,l}$ is set to zero. Thus, resonance effects do not depend on the nanoparticle size a. Accordingly, we shall limit the values of n and l and check the effect on the simulated Raman spectra. In this case, changing the excitation energy or homogeneous broadenings would not modify the relative Raman intensities of the different vibration modes. It would only affect the overall scattering efficiency.

B. Electron-phonon interaction

The electron-phonon interaction is described following the work of Pikus and Bir,[60] who calculated the modulation of the electronic energies and wave functions due to a uniform static strain in the frame of the envelope function formalism. Here, only the first order term of the Hamiltonian, proportional to the dilation, is retained,

$$H_{ph} = D\ \mathrm{div}\ \vec{u}, \tag{13}$$

where $\vec{u}$ is the displacement field and D is the deformation-potential (DP) energy that depends on the considered Bloch function (i.e., on the electronic band).

Hence, the electron-phonon term in Eq. (1) reads

$$\langle \eta_p|H_{ph}|\eta_q\rangle = \langle\Psi_p|\otimes\langle\phi_p|H_{ph}|\phi_q\rangle\otimes|\Psi_q\rangle = \int_{vol} D\zeta^*_{n_p l_p m_p}(\vec{r})\langle\Psi_p|\mathrm{div}\ \vec{u}(\vec{r})|\Psi_q\rangle\zeta_{n_q l_q m_q}(\vec{r})d^3r. \tag{14}$$

In the frame of elasticity theory, $\vec{u}(\vec{r})$ is a continuous displacement field and div $\vec{u}(\vec{r})$ can be evaluated analytically at each point $\vec{r}$ from Eq. (8).

In our atomistic model, the displacement field is discrete by nature and could not rigorously be derived. In order to evaluate the divergence of the displacement, we define a continuous displacement field using

$$\vec{u}(\vec{r}) = A\sum_j \vec{u}(\vec{R}_j)e^{-(\vec{r}-\vec{R}_j)^2/\delta^2} \tag{15}$$

and obtain the divergence term in Eq. (14),

$$\langle\Psi_p|\mathrm{div}\ \vec{u}(\vec{r})|\Psi_q\rangle = \frac{2A}{\delta^2}\sum_j \langle\Psi_p|\vec{u}_j|\Psi_q\rangle\cdot(\vec{R}_j-\vec{r})\exp\left(-\frac{(\vec{r}-\vec{R}_j)^2}{\delta^2}\right). \tag{16}$$

In Eqs. (15) and (16), $\vec{R}_j$ is the equilibrium position of nucleus j, A is a normalization, factor, and δ is a parameter of the order of the interatomic distance (half the interatomic distance in our case). We have checked that the final results are not sensitive to δ as long as realistic values are used. Equation (15) turns the discrete atomic displacements to a continuous field, and, strictly speaking, this cannot be justified. However, such a procedure is standard and has been used to establish Eq. (13) (see Ref. 60). Moreover, that transformation is computationally cheap. It does not create any problem with surface atoms (compared to a divergence calculation based on the Green-Ostrogradski theorem). Terms $\langle\Psi_p|u_{j\alpha}|\Psi_q\rangle$ are calculated from Eq. (A10) (Appendix). In order to fully compare the elasticity theory and the atomistic model, we estimate the effect of evaluating div $\vec{u}$ from Eq. (16) in the frame of Lamb's model. This is performed, on one hand, by calculating analytically div $\vec{u}$ (we will refer to this calculation as the "continuous Lamb" model) and, on the other hand, by calculating div $\vec{u}$ using Eq. (16) (we will then refer to this as the "discrete Lamb" model). The "atomistic model" of Sec. III A 2 inevitably uses Eq. (16).

By turning the continuous integration in Eq. (14) to a discrete sum running over the atomic positions, we obtain

$$\langle\eta_p|H_{ph}|\eta_q\rangle = K\sum_i \zeta^*_{n_p l_p m_p}(\vec{R}_i)\zeta_{n_q l_q m_q}(\vec{R}_i)D\langle\Psi_p|\mathrm{div}\ \vec{u}(\vec{R}_i)|\Psi_q\rangle, \tag{17}$$

where K is a constant[71] and, as a reminder, $|\Psi\rangle$ is a phonon state, and ζ describes the electronic envelop wave functions. Equation (17) directly shows that the electron-phonon coupling is strong if both electronic density and divergence of the displacement field are coincidentally significant.

C. Electron-photon interaction

The electron-photon interaction Hamiltonian in Eq. (1) reads

$$H_\nu = \frac{e\vec{p}\cdot\vec{A}(\vec{r})}{m_e}, \tag{18}$$

where $\vec{A}$ is the vector potential associated with the incident radiation[72] and $\vec{p}$ the electronic momentum operator.

The electron-photon matrix element in Eq. (1) is $\langle \eta_p|H_\nu|\eta_q\rangle = \langle \phi_p|H_\nu|\phi_q\rangle\langle \Psi_p|\Psi_q\rangle$. Using the electronic wave functions $\phi_q(\vec{r}) = \zeta_q(\vec{r})u^q_{Bloch}(\vec{r})$ and retaining only the interband term,[61] one gets

$$\langle \phi_p|H_\nu|\phi_q\rangle = \frac{e\hbar}{im_e}\int\int\int \zeta_p^*(\vec{r})\zeta_q(\vec{r})u^{*p}_{\mathrm{Bloch}}(\vec{r})\vec{\mathrm{grad}}\, u^q_{\mathrm{Bloch}}(\vec{r})\cdot\vec{A}(\vec{r})d^3r. \tag{19}$$

Assuming that $\vec{A}(\vec{r})$ is a slowly varying function on the length scale of the interatomic distance, Eq. (19) can be transformed into the discrete sum,

$$\langle \phi_p|H_\nu|\phi_q\rangle = \sum_i \zeta_p^*(\vec{R}_i)\zeta_q(\vec{R}_i)\vec{I}_{at}\cdot\vec{A}(\vec{R}_i), \tag{20}$$

running over all atoms; $\vec{I}_{at}$ is proportional to the atomic dipole momentum and depends only on the functions $u^{p,q}_{Bloch}(\vec{r})$.

In this work, we are interested in crystals of few nanometers excited at wavelengths $\lambda \gg a$ (a being the nanocrystal radius; λ is typically 500 nm). Hence, the vector potential $\vec{A}(\vec{r})$ inside the nanocrystal is quasiuniform. In this case, off-diagonal terms of the electron-photon interaction are negligible since the electronic wave functions form a set of orthogonal functions [Eq. (20)]. As a consequence, only diagonal terms of the electron-phonon interaction can be responsible for Raman activity [Eq. (1)]. As already discussed in a previous paper,[48] this noticeable size effect has important consequences on the light scattering properties of nanoobjects. For instance, the Raman selection rules are determined by the ability of a given vibration mode to modulate the diagonal terms of the optically excited electronic density. When increasing the size of the nanocrystal, off-diagonal terms of the electron-phonon Hamiltonian come out, whereas diagonal terms cancel.

V. RESULTS

The resonant Raman spectra are simulated using Eq. (1). The latter is calculated using Eqs. (17) and (20). Constants D and K [in Eq. (17)] and $\vec{I}_{at}\cdot\vec{A}$ [in Eq. (20)] are factorized in a proportionality factor. We evaluate the resonant Raman intensity for each vibration mode of the nanocrystal. To allow for a comparison with experiments, the simulated Raman spectra are convolved with a Lorentzian function of 3 cm^{-1} linewidth (typical spectral resolution).

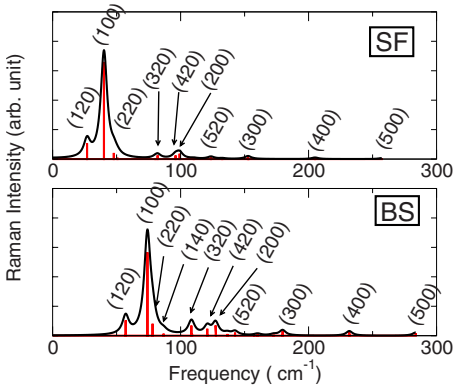

FIG. 1. (Color online) Simulated resonant Raman spectra of a Ge QD with 885 atoms (around 3.5 nm diameter) calculated using the continuous Lamb model for both stress-free (SF) and blocked surface (BS) boundary conditions. The vertical lines show the calculated intensities before convolution with the Lorentzian function.

A. Elasticity theory

1. Convolution effects

We first analyze the Raman activity of the vibration modes calculated using Lamb's model.

Unlike in previous published works,[47,48] here, we report on the Raman activity of not only the pure radial (1,0,0) mode but all spheroidal modes (fundamental and overtones). The excitation wavelength is fixed at $\lambda = 532$ nm close to resonance with the confined E_1 transitions of the germanium nanocrystals. The maximum values of the envelope wave function quantum numbers are fixed at $n_{\max} = 5$ and $l_{\max} = 5$ [see Eq. (11)].

Figure 1 presents convolved and unconvolved Raman spectra of a germanium QD (885 atoms) calculated using Lamb's model for both stress-free and blocked surface boundary conditions. Comparing the convolved and unconvolved spectra in Fig. 1 allows one to identify the vibration modes that could be observed experimentally in the Raman spectra and which modes do contribute to a single Raman peak. The relative Raman intensities of the different Lamb modes are reported in Table I for stress-free boundary conditions.

We found that the Raman active Lamb modes have an even value of l, as observed experimentally.[11,16,62] This is in agreement with the predictions reported years ago by Duval,[63] who used a qualitative analysis of the light scattering process based on the rotation group symmetry. It is worthwhile to underline that here no assumption is made concerning the Raman selection rules. The Raman activity of the vibration modes comes out as a result of the simulations. It is a direct consequence of the optically excited electronic states and their modulation by the deformation fields via DP interaction. Moreover, our results disagree with a recent publication by Kanehisha[64] (see also Goupalov *et al.*[65]) who proposed that vibration modes with odd l are the Raman active modes, whereas those with even l should be observed by means of infrared absorption. This prediction was based on qualitative arguments which did not take into account the

TABLE I. Raman active Lamb modes of a 885 atoms Ge QD with stress-free boundary conditions. The relative intensities are normalized with respect to the intensity of mode (100).

Mode frequency (cm^{-1})	Relative Raman intensity	Lamb mode (nlm)
26.89	0.16	(1, 2, 0)
40.13	1	(1, 0, 0)
47.82	0.063	(2, 2, 0)
50.67	0.014	(1, 4, 0)
80.26	0.007	(2, 4, 0)
82.04	0.038	(3, 2, 0)
96.07	0.037	(4, 2, 0)
99.25	0.055	(2, 2, 0)
110.25	9.4×10^{-6}	(3, 4, 0)
123.72	0.020	(5, 2, 0)
132.52	2.4×10^{-6}	(4, 4, 0)
152.55	0.022	(3, 0, 0)
205.04	0.014	(4, 4, 0)
257.23	8.51×10^{-3}	(5, 5, 0)

explicit form of the electron-phonon interaction Hamiltonian. The symmetry of a vibration mode is not sufficient to determine its Raman activity.

Coming back to Fig. 1, one has to notice that the Raman spectra due to Lamb's modes are discrete. This is a consequence of the size induced quantization of the vibration eigenmodes.[66] Moreover, a strong peak in the convolved Raman spectra can have two different origins. It corresponds either to the scattering by a single vibration mode with a strong Raman activity or to that by several unresolved modes. This is particularly important for the interpretation of the measured low-frequency Raman signal.

Since the number of vibration modes calculated using Lamb's model is rather small, only few modes contribute to the Raman peaks in Fig. 1. For instance, only the fundamental radial ($l=0$) and quadrupolar ($l=2$) modes do contribute to the most intense Raman peak. The contribution of the (1,2,0) mode is one order of magnitude smaller than that of the (1,0,0) mode because of the weaker dilation field associated with quadrupolar vibrations.

As will be shown later, the effect of the vibration density of states is more important for the atomistic description since all vibration modes are involved in the light scattering: typically, thousands of vibration eigenmodes distributed on few hundreds of wave numbers.

2. Discretization effects

This subsection discusses the effects of the continuous displacement field introduced by Eq. (15) on the simulated Raman spectra and on the comparison between the elasticity theory and the atomistic description.

Figure 2 presents the Raman spectra of a QD (885 atoms) calculated using both continuous and discrete Lamb models for both stress-free and blocked surface boundary conditions. The only difference between these two models lies in the evaluation of the deformation field associated with each vibration mode. In the low-frequency range (0–90 cm^{-1}), the Raman spectra calculated using the discrete Lamb model agree well with the spectra generated with the continuous Lamb model. At higher frequencies, some differences are visible due to the fact that the wavelengths of high-frequency vibrations [see Eq. (9)] become comparable to the interatomic distances [Eq. (10)] and thus our discrete description naturally fails.

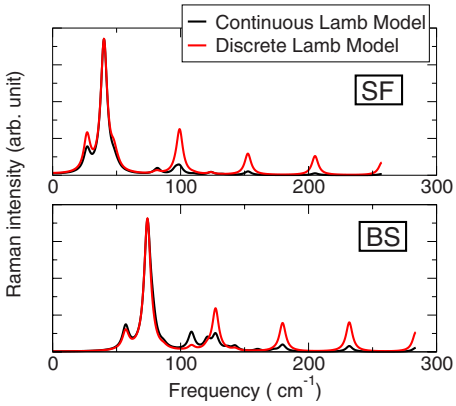

FIG. 2. (Color online) Resonant Raman spectra of a 885 atom Ge QD simulated using the continuous Lamb model and the discrete Lamb model for both SF and BS boundary conditions. The spectra are convolved by a Lorentzian function.

The comparison presented in Fig. 2 validates the calculation procedure of the displacement vector divergence for the atomistic description at low-frequency (below 90 cm^{-1}). In the following, we shall focus on the comparison between the continuous Lamb model and the atomistic model.

B. Atomistic description

The atomistic description allows us to determine all vibration modes, including optical modes contrary to Lamb's theory. Moreover, in the atomistic description, the crystal anisotropy and the presence of inhomogeneities (e.g., alloying effects[67] and strain relaxation effects) are taken into account. In particular, the surface modes come out naturally. The cost to pay for that is the large computational time: For a QD containing N atoms, a $3N\times3N$ dynamical matrix has to be diagonalized and produces a $3N\times3N$ transfer matrix P. Quantum dots containing up to 1800 atoms are studied in this work.

Figure 3 shows the vibration density of states and resonant Raman spectra of a 885 atom QD simulated for both stress-free and blocked surface boundary conditions. The calculations were performed for both acoustic and optical vibration modes. However, the latter are not visible in the Raman spectra because their interaction with confined electrons (and holes) via the DP mechanism is strong only when the wavelength of the excited electronic states is comparable to the vibration wavelengths, i.e., for envelope wave functions associated with large n or l. Since we used limited values of n and l, optical vibration modes do not show a realistic Raman activity. Increasing n and l would not help because the para-

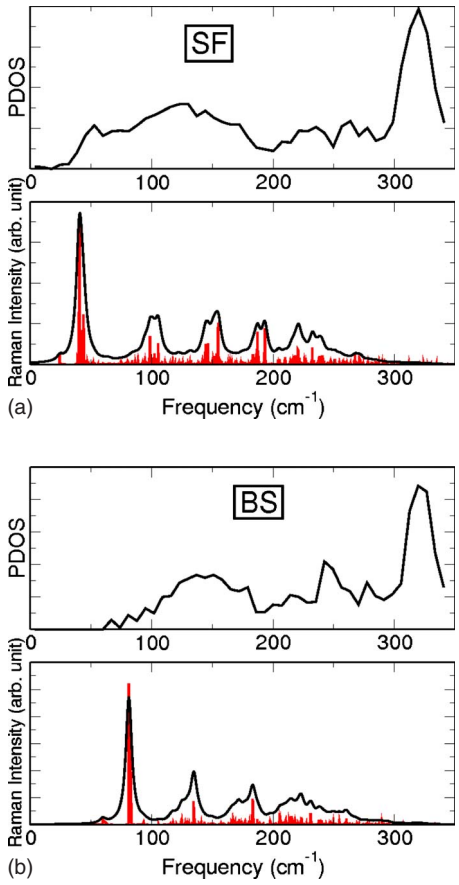

FIG. 3. (Color online) Vibration density of states and resonant Raman spectra of a spherical Ge QD consisting of 885 atoms. Both convolved and unconvolved Raman spectra are shown. The upper graph refers to the SF boundary conditions, and the lower graph to the BS boundary conditions.

bolic band approximation is not valid for large quantum numbers. In addition, the calculation procedure of the displacement field divergence is not suitable for high-frequency vibration modes, as shown in Fig. 2. Hence, only the low-frequency range (0–90 cm^{-1}) is relevant in Fig. 3. Thereafter, we shall focus on the low-frequency Raman scattering due to acoustic vibration modes only.

As already mentioned above, the atomistic description gives a complete set of vibration eigenmodes. With increasing number of atoms (particle size), the vibration eigenfrequencies form a quasicontinuum. This quasicontinuous spectrum could be responsible for strong Raman peaks in the convolved spectrum (see, for instance, the low-frequency lines in Fig. 3). The atomistic description can thus indicate whether a strong Raman intensity is due to a single very active vibration mode or, rather, to a high density of fairly active modes.

C. Comparison of atomistic and Lamb theories

Figure 4 shows resonant Raman spectra of a 885 atom Ge QD simulated for free and blocked surface boundary conditions. The vibration eigenmodes were calculated in the frame

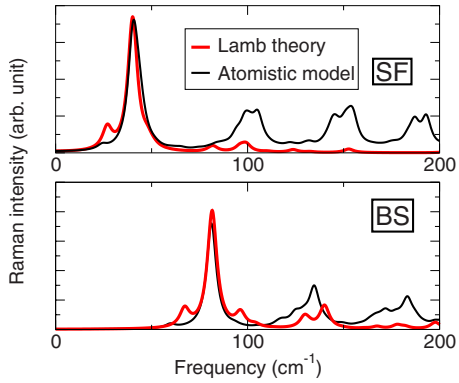

FIG. 4. (Color online) Simulated resonant Raman spectra of a Ge QD consisting of 885 atoms. The vibration eigenvectors are calculated using either Lamb's model or the atomistic description. Both SF and BS boundary conditions are considered.

of both the atomistic description and elasticity theory.

First, the Raman lines calculated using Lamb's model and the atomistic model do not occur at exactly the same frequencies. However, the agreement between the two models is very good considering that the anisotropy of the sound velocities is not taken into account in Lamb's model:[16] Here, directionally averaged sound velocities were used.

Above 100 cm^{-1} (Fig. 4), the Raman intensity generated with the atomistic model is larger than that calculated with Lamb's model. As already discussed, the calculation of the displacement vector divergence becomes questionable for this frequency range (see Fig. 2). Moreover, above 100 cm^{-1}, the phonon density of states is very high (see Fig. 3), leading to cumulative numerical errors in the convolved Raman spectra. Hence, we shall focus our discussion on the lowest frequency range, which is usually investigated in experiments.[11,16,62]

In order to compare quantitatively Lamb's model and the atomistic model, we project the Raman active vibration eigenmodes of the atomistic description on Lamb's modes following the work of Cheng *et al.*[36] Let $\vec{u}^n_{atom}$ be the nth vibration mode of the atomistic model and $\vec{u}^j_{Lamb}$ the jth mode of Lamb's model (n and j being a set of quantum numbers); the mode projection quantity (MPQ) R_{nj} reads

$$R_{nj} = \left[\sum_{position} \vec{u}^n_{atom} \cdot \vec{u}^j_{Lamb} \right]^2. \tag{21}$$

By projecting atomistic modes on Lamb modes, it is possible to evaluate the "Lamb character" of each atomistic mode. Table II sums up the mode character analysis for the first two vibration eigenmodes of the atomistic model responsible for the lowest frequency peak in Fig. 3. The table only refers to the case of stress-free boundary conditions. The same qualitative conclusions are found for blocked surface boundary conditions. Notice that, by construction, Lamb modes are orthonormalized for the continuous scalar product $\langle \vec{u}^i | \vec{u}^j \rangle = \int\int\int \vec{u}^i(\vec{R}) \cdot \vec{u}^j(\vec{R}) d^3R$ and not for the discrete one $\langle \vec{u}^i | \vec{u}^j \rangle = \Sigma_n \vec{u}^i_{R_n} \cdot \vec{u}^j_{R_n}$, so that the sum of the MPQs for a given atomistic modes on Lamb modes may differ from 1.

TABLE II. MPQ of the first two atomistic vibration eigenmodes on the pure radial and quadrupolar Lamb modes. These modes give rise to the main Raman peaks in Fig. 4.

Atomistic mode frequency (cm^{-1})	Lamb mode (n,l,m) frequency (cm^{-1})	MPQ
	(1, 2, 0) [26.89]	0.44
	(2, 2, 0) [47.82]	0.46
24.23	(3, 2, 0) [82.04]	0.30
	(4, 2, 0) [96.07]	0.38
	(5, 2, 0) [123.72]	0.36
40.25	(1, 0, 0) [40.13]	0.52

From Table II, one can see that the vibration modes calculated in the frame of the atomistic model project on several Lamb's modes. The first two Raman active modes of the atomistic model, which contribute to the strong low-frequency Raman peak (shoulder at 40.25 cm^{-1} and peak at 24.23 cm^{-1} in Fig. 3 SF), involve the fundamental pure radial (1,0,0) and quadrupolar (fundamental and overtones) modes $(n,2,0)$.

The peak at 40.25 cm^{-1} is composed mainly of the (1,0,0) mode as attested by the corresponding MPQ=0.52. MPQ on other Lamb modes are smaller than 0.05. This result complements the work of Cheng *et al.*[36] By projecting Lamb's modes on atomistic ones, they conclude that the Lamb mode (1,0,0) is composed of more than one lattice mode when particle diameters become smaller than 4 nm.

Notice that despite its rather high frequency (123.72 cm^{-1}), the overtone mode (5,2,0) has a significant contribution to the weak shoulder at 24.23 cm^{-1}, as indicated by the corresponding MPQ=0.36. We have increased the number of Lamb modes onto which the atomistic modes are projected. We found that the projection of the atomistic mode at 24.23 cm^{-1} on the Lamb mode (6,2,0) is very weak (MPQ=0.02). Hence, Table II gives the main Lamb decomposition of the first two atomistic modes.

One can notice in Fig. 4 that the Raman intensity of the quadrupolar mode is smaller when using the atomistic model. Indeed, with Lamb's model and for stress-free boundary conditions, it is about 16% (see Table I) of the breathing mode intensity. On the other hand, in the atomistic model, it falls to 6.4%. In the case of fixed boundary conditions, it decreases from 18% (Lamb) to only 2.8% (atomistic).

Therefore, though the agreement between the low-frequency Raman spectra simulated with the atomistic model and the Lamb model is good (as shown in Fig. 4), the Raman active vibration modes differ but have mainly the same symmetry (pure radial or quadrupolar).

D. Size effects

Figure 5 shows the size dependence of the Raman spectra simulated using both Lamb's model and the atomistic model for both stress-free and blocked surface boundary conditions. Figure 6 reports the frequencies of the first two atomistic modes (see Table II) responsible for the lowest frequency Raman peak. These modes are labeled $(n,2,0)$ and (1,0,0) according to their projection on Lamb's modes (Table II). In the spectra simulated using Lamb's modes, the lowest frequency Raman peak is due to the (1,2,0) and (1,0,0) modes (Fig. 1). Their vibration frequencies are plotted in Fig. 6 as a function of the QD size.

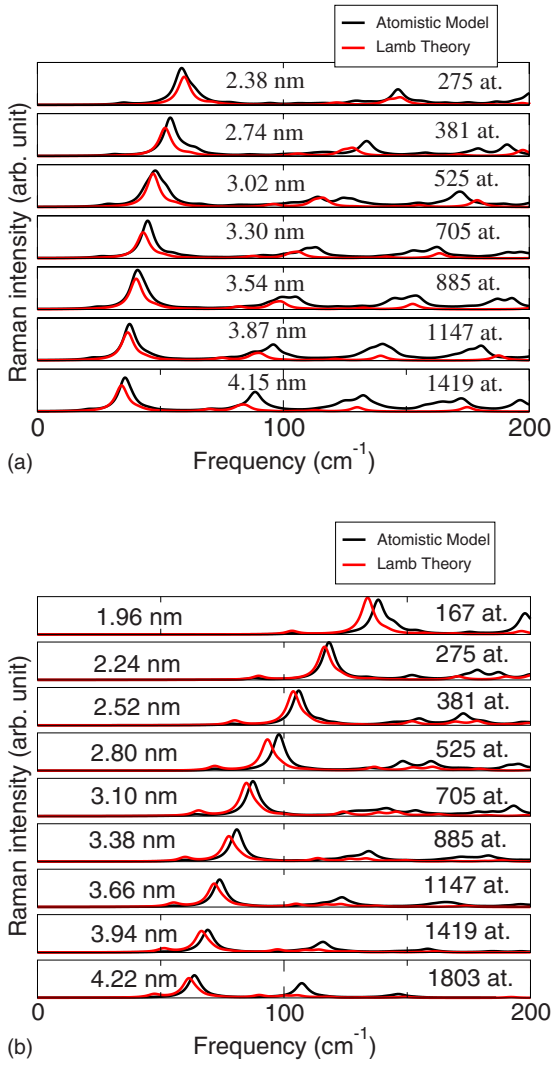

FIG. 5. (Color online) Resonant Raman spectra simulated using vibration eigenmodes from Lamb's model and from the atomistic model for both stress-free (lower panel) and rigid (upper panel) surface boundary conditions. The quantum dot diameter is indicated for each plot.

It is well known that the frequencies of Lamb's modes scale as the inverse of the nanoparticle diameter. This result could easily be deduced from Eq. (8). It has been used to extract from the low-frequency Raman data the average size and size dispersion of semiconductor and metal nanoparticles.[11,16,62,68] The comparison with the frequencies of the (1,0,0) and $(n,2,0)$ atomistic modes shows that this law is well verified.

For the pure radial and quadrupolar vibrations, the frequency shift between Lamb's and atomistic modes does not exceed 3.5 cm^{-1} for a free particle surface and 4 cm^{-1} for a

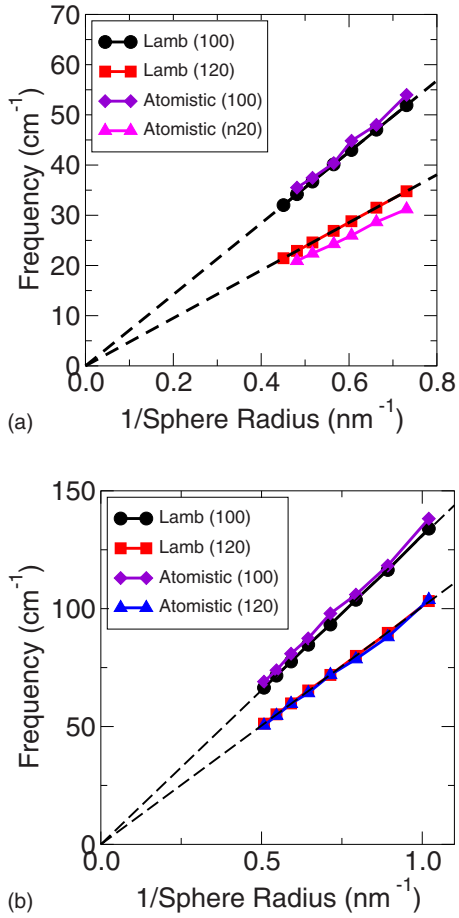

FIG. 6. (Color online) Frequencies of the first two Raman active modes as a function the inverse QD radius. Dashed lines are linear regressions for the two Lamb modes.

fixed particle surface. This difference between the vibration frequencies comes from the definition of the diameter of the spherical QD. Here, the radius is defined by the distance between the mass center and the most distant atom plus half the lattice parameter in the case of free surface boundary and by the distance between the mass center and the most distant atom in the case of blocked surface. Since the frequencies of Lamb's modes scale as the inverse of the QD radius, they are sensitive to the exact definition of this parameter especially in the case of very small QDs.

Our calculations show that even for a particle diameter less than 4nm, the *frequencies* of Lamb's and atomistic modes are very similar. Hence, Lamb's theory still gives a good approximation of the vibration frequencies. This is surprising since, as it has been shown by Cheng *et al.*,[35] the description of QD vibration modes in terms of Lamb's modes breaks down for a particle diameter smaller than 4 nm. Our analysis of the Raman spectra and Fig. 6, in particular, show that though Lamb's model breaks for small diameters, the frequencies of the Raman active modes go on scaling as the inverse of the QD size at least for diameters larger than 2.38 nm. This point will be discussed below.

VI. DISCUSSION AND MODEL VALIDITY

A. Electronic eigenstates

As already mentioned, the envelope function approximation is unable to describe the electronic properties of QD having less than 200 atoms. First-principles calculations would be more suitable (but also more expensive in computation). Moreover, we assume that the nanoparticle behaves as an infinitely deep potential well: vanishing envelope wave functions at the QD surface. This assumption is certainly not true for very small QDs. The electronic states could extend out of the QD depending on the QD/matrix band offset.[46] Such effects would modify the Raman activity of the vibration modes, as discussed in Sec. IV B.

Despite these limitations, the envelope wave function approximation allows one to generate resonant Raman spectra of QD vibration modes in a rather simple way and allows precise comparison with experiments.[48]

B. Vibration eigenstates

In our analysis of the Raman scattering and for the comparison with the atomistic model, we have considered a limited number of (n,l,m) Lamb modes (maximum n is 5, though this number should be extended further[66]). Actually, from Eq. (17), vibration modes and electronic wave functions interact efficiently, provided their spatial variation occurs on the same length scale (i.e., similar wavelengths). Therefore, since we used a limited number of electronic states (in order to keep within the effective mass approximation), we have also used a limited number of vibration Lamb modes. However, we checked that increasing the number of Lamb modes (as well as increasing the number of electronic eigenstates) does not modify the Raman spectra in the low-frequency range (quadrupolar and breathing mode Raman activity).

Moreover, the semiempirical potential of SW becomes a poor approximation for very small QDs (less than a hundred atoms). The structural and the vibrational properties are certainly not described correctly. Especially, one of the major drawbacks of the SW potential is that it fails to model the surface relaxation (surface stress) since it involves only nearest neighbor interaction. Surface relaxation typically involves atoms at two or three atomic distances (of the order of the interaction range between atoms) in the vicinity of the surface. Since the effect of the surface relaxation on structural and phonon properties is proportional to the surface/volume ratio, we expect a significant effect of the surface stress on the vibrational properties for very small QDs.[69] Using the SW potential, we do not probe these surface stress effects, but we investigate confinement effects of vibration modes. This is why the frequencies of the quadrupolar and breathing modes in Fig. 6 inversely scales as the QD size in our atomistic simulations. The particle size becomes the main characteristic length of the problem (the other one is the interatomic distance).

VII. CONCLUSION

We have reported the first attempt to couple an atomistic description of QD vibration modes to a quantum description

of the resonant Raman scattering. The resonant optical excitation of confined electronic transitions is usually used to overcome the low scattering efficiency of QDs. Thus, a complete modeling of the resonant light scattering process is needed for the interpretation of experiments. Moreover, the Raman spectra simulated with the Lamb and atomistic SW vibration modes were compared. Unlike in a previous work,[48] we have not restricted the discussion to a single particular Lamb mode. All spheroidal vibration eigenmodes were considered.

Our main findings can be summarized as follows: (i) We found a good agreement between the vibration frequencies of acoustic modes calculated using Lamb's model and the atomistic approach. For a surface-free QD, the frequency shift of the radial and quadrupolar Lamb modes (1,0,0) and (1,2,0), with respect to the corresponding atomistic modes, is smaller than 3.5 cm^{-1} for a QD diameter larger than 2.38 nm (i.e., a 275 atom QD). (ii) In the atomistic SW model, the vibration modes that are responsible for the main low-frequency Raman peak, usually observed in experiments, project principally onto the pure radial and quadrupolar Lamb modes (fundamental and overtones). This confirms the interpretations of the low-frequency Raman scattering in semiconductor quantum dots based on Lamb's model, and disagrees with recently suggested revisions.[64] (iii) In the frame of the deformation-potential coupling mechanism, we found that the radial mode (1,0,0) gives the dominant contribution to the low-frequency Raman signal, as observed experimentally for some semiconductor QDs.[11,48,62,70] The weaker Raman activity of the quadrupolar mode (1,2,0) is due to the smaller volume change associated with this type of vibrations. However, the relative contribution of the radial and quadrupolar modes strongly depends on the coupling mechanism between the QD vibration modes and electronic states, i.e., on the semiconductor or metallic nature of the QD.[68]

APPENDIX: NORMALIZATION OF EIGENVIBRATIONAL MODE

Starting from the Hamiltonian,

$$H_0^{\mathcal{N}} = \sum_{l=0}^{3N-1} \left[\frac{\Pi_l^2}{2} + \frac{\Omega_l^2}{2}\Theta_l^2 \right]. \tag{A1}$$

The eigenstate $|\Psi\rangle$ of $H_0^{\mathcal{N}}$ can be written as a tensorial product of eigenstates $|\Psi_{n_l}\rangle$ of harmonic oscillators, n_l being the number of quanta in vibration mode l,

$$|\Psi(n_0, n_1 \cdots n_{3N-1})\rangle = |\Psi_{n_0}\rangle \otimes \cdots \otimes |\Psi_{n_{3N-1}}\rangle. \tag{A2}$$

We have the well-known relations

$$\Theta_l = \sqrt{\frac{\hbar}{2\Omega_l}}(a_l^\dagger + a_l), \tag{A3}$$

$$a_l|\Psi_{n_l}\rangle = \sqrt{n_l}|\Psi_{n_l-1}\rangle, \tag{A4}$$

$$a_l^\dagger|\Psi_{n_l}\rangle = \sqrt{n_l+1}|\Psi_{n_l+1}\rangle, \tag{A5}$$

$$H_0^{\mathcal{N}} = \sum_{l=0}^{3N-1} \hbar\Omega_l\left(a_l^\dagger a_l + \tfrac{1}{2}\right), \tag{A6}$$

where $a_l^\dagger$ and a_l are, respectively, the creation and annihilation operators of vibration mode l.

The displacement operator of nucleus i in direction α ($l=3i+\alpha$) reads

$$u_l = \frac{u_l'}{\sqrt{m_l}} \tag{A7}$$

$$= \sum_{k=0}^{3N-1} P[l,k]\sqrt{\frac{\hbar}{2\Omega_k m_l}}(a_k^\dagger + a_k). \tag{A8}$$

In the following, we evaluate matrix elements of the form $\langle\Psi_p|u_{i\alpha}|\Psi_q\rangle$ for a given atom i. This task becomes easy using Eq. (A8) and the vibration eigenstates, $|\Psi_q\rangle = |\Psi_{n_0^q}\rangle \otimes \cdots \otimes |\Psi_{n_{3N-1}^q}\rangle$,

$$\langle\Psi_p|u_l|\Psi_q\rangle = \left\langle \Psi_p \left| \sum_{k=0}^{3N-1} P[l,k]\sqrt{\frac{\hbar}{2\Omega_k m_l}}(a_k^\dagger + a_k) \right| \Psi_q \right\rangle \tag{A9}$$

$$= \left\langle \Psi_p \left| \sum_{k=0}^{3N-1} P[l,k]\sqrt{\frac{\hbar}{2\Omega_k m_l}}\sqrt{n_k^q+1} \right| \Psi_{n_0^q} \right\rangle \otimes \cdots |\Psi_{n_k^q+1}\rangle \cdots \otimes |\Psi_{n_{3N-1}^q}\rangle + \left\langle \Psi_p \left| \sum_{k=0}^{3N-1} P[l,k]\sqrt{\frac{\hbar}{2\Omega_k m_l}}\sqrt{n_k^q} \right| \Psi_{n_0^q} \right\rangle \otimes \cdots |\Psi_{n_k^q-1}\rangle \cdots \otimes |\Psi_{n_{3N-1}^q}\rangle. \tag{A10}$$

This matrix element is different from zero in two cases.

$|\Psi_p\rangle$ must read

$$|\Psi_p\rangle = |\Psi_{n_0^q}\rangle \otimes \cdots |\Psi_{n_k^q-\epsilon}\rangle \cdots \otimes |\Psi_{n_{3N-1}^q}\rangle. \tag{A11}$$

With $\epsilon=-1$, which corresponds to the creation of a quantum vibration in the eigenmode k,

$$\langle\Psi_p|u_{i\alpha}|\Psi_q\rangle = P[l,k]\sqrt{\frac{\hbar}{2\Omega_k m_l}}\sqrt{n_k^q+1}. \tag{A12}$$

with $\epsilon=1$, corresponding to the annihilation of such a quantum,

$$\langle\Psi_p|u_{i\alpha}|\Psi_q\rangle = P[l,k]\sqrt{\frac{\hbar}{2\Omega_k m_n}}\sqrt{n_k^q}. \tag{A13}$$

The mean value of n_k^q is given by the Bose distribution,

$$n_k^q = \frac{1}{e^{-\hbar\Omega_k/k_BT}-1}, \tag{A14}$$

where k_B is the Boltzmann constant and T the temperature.

Moreover, normalization of the vibration eigenmodes is performed using the condition $P^tP=I$ so that

$$\sum_{k=0}^{3N-1} P[k,l']P[k,l] = \delta_{ll'}. \quad \text{(A15)}$$

From Eq. (A7), $u_k^l = P[k,l]/\sqrt{m_k}$ is the displacement of atom i in the vibration eigenmode l along the direction α with $k = 3i+\alpha$. Thus, in a classical approach, as for the Lamb theory, Eq. (A15) becomes

$$\sum_{k=0}^{3N-1} \sqrt{m_k}u_k^{l'}\sqrt{m_k}u_k^l = \delta_{ll'}. \quad \text{(A16)}$$

The continuous formulation of this equation reads

$$\int \rho(\vec{r})\vec{u}^l(\vec{r})\vec{u}^{l'}(\vec{r})d^3r = \delta_{ll'}, \quad \text{(A17)}$$

where $\rho(\vec{r})$ is the mass density.

*combe@cemes.fr
†Present address: Groupe d'Etude des Semiconducteurs, UMR 5650 CNRS-Université Montpellier II Bat 21, CC074, Place Eugène Bataillon, 34095 Montpellier Cedex 05, France; jean-roch.huntzinger@univ-montp2.fr
‡adnen.mlayah@cemes.fr

[1] D. Kopev, D. Mirlin, V. Sapega, and A. Sirenko, JETP Lett. **51**, 708 (1990).
[2] V. Sapega, V. Belitsky, A. J. Shields, T. Ruf, M. Cardona, and K. Ploog, Solid State Commun. **84**, 1039 (1992).
[3] J. R. Huntzinger, J. Groenen, M. Cazayous, A. Mlayah, N. Bertru, C. Paranthoen, O. Dehaese, H. Carrère, E. Bedel, and G. Armelles, Phys. Rev. B **61**, R10547 (2000).
[4] M. Cazayous, J. R. Huntzinger, J. Groenen, A. Mlayah, S. Christiansen, H. P. Strunk, O. G. Schmidt, and K. Eberl, Phys. Rev. B **62**, 7243 (2000).
[5] M. Cazayous, J. Groenen, J. R. Huntzinger, A. Mlayah, and O. G. Schmidt, Phys. Rev. B **64**, 033306 (2001).
[6] M. Cazayous, J. Groenen, A. Zwick, A. Mlayah, R. Carles, J. L. Bischoff, and D. Dentel, Phys. Rev. B **66**, 195320 (2002).
[7] A. Milekhin, A. I. Nikiforov, O. P. Pchelyakov, S. Schulze, and D. R. T. Zhan, JETP Lett. **73**, 461 (2001).
[8] A. G. Milekhin, A. Nikiforov, O. P. Pchelyakov, S. Schulze, and D. Zhan, Nanotechnology **13**, 55 (2002).
[9] A. G. Milekhin, A. Nikiforov, O. P. Pchelyakov, S. Schulze, and D. Zhan, Physica E (Amsterdam) **13**, 582 (2002).
[10] H. Kushibe, M. Nakayama, and M. Yokota, Phys. Rev. B **47**, 9566 (1993).
[11] A. Tanaka, S. Onari, and T. Arai, Phys. Rev. B **47**, 1237 (1993).
[12] A. Othmani, C. Bouvier, J. C. Plenet, J. Dumas, B. Champagnon, and C. Mai, Mater. Sci. Eng., A **168**, 263 (1993).
[13] L. Saviot, B. Champagnon, E. Duval, and A. I. Ekimov, Phys. Rev. B **57**, 341 (1998).
[14] M. Fujii, Y. Kanzawa, S. Hayashi, and K. Yamamoto, Phys. Rev. B **54**, R8373 (1996).
[15] M. Pauthe, E. Berstein, J. Dumas, L. Saviot, A. Pradel, and M. Ribes, J. Mater. Chem. **9**, 187 (1999).
[16] L. Saviot, D. B. Murray, and M. C. Marco de Lucas, Phys. Rev. B **69**, 113402 (2004).
[17] M. Ivanda, A. Holh, M. Montagna, G. Marioto, M. Ferrari, Z. C. Orel, A. Turković, and K. Furić, J. Raman Spectrosc. **37**, 161 (2006).
[18] N. N. Ovsyuk, E. B. Orokhov, V. V. Grishchenko, and A. Shabanin, JETP Lett. **47**, 298 (1988).
[19] Y. M. Yang, X. L. Wu, L. W. Yang, G. S. Hunag, G. G. Siu, and P. K. Chu, J. Appl. Phys. **98**, 064303 (2005).
[20] P. K. Giri, R. Kesavamoorthy, B. K. Panigrahi, and K. G. M. Nair, Solid State Commun. **136**, 36 (2005).
[21] M. Fujii, T. Nagareda, S. Hayashi, and K. Yamamoto, Phys. Rev. B **44**, 6243 (1991).
[22] G. Mariotto, M. Montagna, E. D. G. Viliani, S. Lefrant, E. Rzepka, and C. Mai, Europhys. Lett. **6**, 239 (1988).
[23] B. Palpant, H. Portales, L. Saviot, J. Lermé, B. Prével, M. Pellarin, E. Duval, A. Perez, and M. Broyer, Phys. Rev. B **60**, 17107 (1999).
[24] E. Duval, H. Portales, L. Saviot, M. Fujii, K. Sumitomo, and S. Hayashi, Phys. Rev. B **63**, 075405 (2001).
[25] H. Portales, L. Saviot, E. Duval, M. Fujii, S. Hayashi, N. D. Fatti, and F. Vallee, J. Chem. Phys. **115**, 3444 (2001).
[26] A. Courty, I. Lisiecki, and M. P. Pileni, J. Chem. Phys. **116**, 8074 (2002).
[27] L. Saviot and D. B. Murray, Phys. Rev. Lett. **93**, 055506 (2004).
[28] D. A. Weitz, T. J. Gramila, A. Z. Genack, and J. I. Gersten, Phys. Rev. Lett. **45**, 355 (1980).
[29] J. I. Gersten, D. A. Weitz, T. J. Gramila, and A. Z. Genack, Phys. Rev. B **22**, 4562 (1980).
[30] E. Duval, A. Boukenter, and B. Champagnon, Phys. Rev. Lett. **56**, 2052 (1986).
[31] A. Tamura and T. Ichinokawa, J. Phys. C **16**, 4779 (1983).
[32] A. Tanguy, J. P. Wittmer, F. Leonforte, and J.-L. Barrat, Phys. Rev. B **66**, 174205 (2002).
[33] F. Leonforte, A. Tanguy, J. P. Wittmer, and J.-L. Barrat, Phys. Rev. B **70**, 014203 (2004).
[34] F. Leonforte, R. Boissière, A. Tanguy, J. P. Wittmer, and J.-L. Barrat, Phys. Rev. B **72**, 224206 (2005).
[35] W. Cheng and S. F. Ren, Phys. Rev. B **65**, 205305 (2002).
[36] W. Cheng, S. F. Ren, and P. Y. Yu, Phys. Rev. B **71**, 174305 (2005).
[37] W. Cheng, S. F. Ren, and P. Y. Yu, Phys. Rev. B **68**, 193309 (2003).
[38] R. Alben and D. Weaire, Phys. Rev. B **11**, 2271 (1975).
[39] R. J. Bell, *Methods in Computational Physics* (Academic, New York, 1976), Vol. 15, p. 260.
[40] R. Saito, T. Takeya, T. Kimura, G. Dresselhaus, and M. S. Dresselhaus, Phys. Rev. B **57**, 4145 (1998).
[41] S. Guha, J. Menéndez, J. B. Page, and G. B. Adams, Phys. Rev. B **53**, 13106 (1996).
[42] B. Zhu and K. A. Chao, Phys. Rev. B **36**, 4906 (1987).
[43] M. G. Burt, J. Phys.: Condens. Matter **11**, R53 (1999).
[44] P. Harrison, *Quantum Wells, Wires and Dots*, 2nd ed. (Wiley, Chichester, 2006).
[45] A. A. Sirenko, V. I. Belitsky, T. Ruf, M. Cardona, A. I. Ekimov,

and C. Trallero-Giner, Phys. Rev. B **58**, 2077 (1998).
[46] M. P. Chamberlain, C. Trallero-Giner, and M. Cardona, Phys. Rev. B **51**, 1680 (1995).
[47] S. V. Gupalov and I. A. Merkulov, Phys. Solid State **41**, 1349 (1999).
[48] J. R. Huntzinger, A. Mlayah, V. Paillard, A. Wellner, N. Combe, and C. Bonafos, Phys. Rev. B **74**, 115308 (2006).
[49] P. Yu and M. Cardona, *Fundamentals of Semiconductors* (Springer, Berlin, 1996).
[50] D. L. Andrews, S. Naguleswaran, and G. E. Stedman, Phys. Rev. A **57**, 4925 (1998).
[51] H. Lamb, Proc. London Math. Soc. **13**, 187 (1882).
[52] F. H. Stillinger and T. A. Weber, Phys. Rev. B **31**, 5262 (1985).
[53] F. H. Stillinger and T. A. Weber, Phys. Rev. B **33**, 1451 (1986).
[54] M. Laradji, D. P. Landau, and B. Dünweg, Phys. Rev. B **51**, 4894 (1995).
[55] R. Vink, G. Barkema, W. V. der Weg, and N. Mousseau, J. Non-Cryst. Solids **282**, 248 (2001).
[56] A. Huang, *Theoretical Solid State Physics*, 1st ed. (D. Ter Haar, Oxford, 1972).
[57] M. Cardona and F. H. Pollak, Phys. Rev. **142**, 530 (1966).
[58] F. H. Pollak and M. Cardona, Phys. Rev. **172**, 816 (1968).
[59] J. L. Pan, Phys. Rev. B **46**, 4009 (1992).
[60] G. E. Pikus and G. L. Bir, Sov. Phys. Solid State **1**, 1502 (1960).
[61] G. Bastard, *Wave Mechanics Applied to Semiconductor Heterostructures*, 1st ed. (Wiley, Chichester, 1991).
[62] P. Verma, W. Cordts, G. Irmer, and J. Monecke, Phys. Rev. B **60**, 5778 (1999).
[63] E. Duval, Phys. Rev. B **46**, 5795 (1992).
[64] M. Kanehisa, Phys. Rev. B **72**, 241405(R) (2005).
[65] S. V. Goupalov, L. Saviot, and E. Duval, Phys. Rev. B **74**, 197401 (2006).
[66] A. Tamura, Phys. Rev. B **52**, 2668 (1995).
[67] S.-F. Ren, W. Cheng, and P. Y. Yu, Phys. Rev. B **69**, 235327 (2004).
[68] G. Bachelier and A. Mlayah, Phys. Rev. B **69**, 205408 (2004).
[69] A. Tamura, K. Higeta, and T. Ichinokawa, J. Phys. C **15**, 4975 (1982).
[70] M. Ivanda, K. Babocsi, C. Dem, M. Schmitt, M. Montagna, and W. Kiefer, Phys. Rev. B **67**, 235329 (2003).
[71] This prefactor is of the order of the volume per atom. It is due to our discretization, and we did not gather both the deformation potential D and K in a single prefactor at this point for pedagogical reasons.
[72] To be replaced by its complex conjugate $\vec{A}^*$ for the scattered radiation.